Controls of riverine CO_2 over an annual cycle determined using direct, high temporal resolution pCO_2 measurements

Janet K. Lynch,[1] Cory M. Beatty,[1] Matthew P. Seidel,[1] Laura J. Jungst,[1] and Michael D. DeGrandpre[1]

Received 25 August 2009; revised 2 March 2010; accepted 19 March 2010; published 12 August 2010.

[1] Autonomous CO_2 sensors were deployed in the Clark Fork River, Montana, USA, to characterize the partial pressure of CO_2 (pCO_2) during an annual cycle. A total of 23,941 measurements were made spanning the period 2002–2006. These data were compiled into a composite data set covering ~309 days, giving an unprecedented yearlong view of the carbon cycle dynamics of a riverine system. Seasonal pCO_2 varied from a winter minimum of ~100 μatm to a fall maximum of ~900 μatm. The pCO_2 changed by as much as 460 μatm during a diel period, much larger than the range of the seasonal mean, in contrast to most other aquatic ecosystems where seasonal variability dominates. The diel pCO_2 amplitude was primarily controlled by the net ecosystem production (NEP) throughout the year, although heating/cooling and air-water exchange significantly altered the diel pCO_2 (and pH) magnitude. Although infrequent, rain events contributed ~21% to the cumulative short-term changes in inorganic carbon through CO_2-enriched runoff. The seasonal cycle was controlled by temperature, NEP, and discharge. The Clark Fork River maintained pCO_2 levels that were supersaturated with respect to the atmosphere for the majority of the year. River-to-atmosphere CO_2 gas exchange was estimated to be between 4.7 and 7.1 mol C m^{-2} yr^{-1}. The loss of CO_2 to the atmosphere arises from net heterotrophy that averaged 13.8 mmol m^{-2} d^{-1}. The time series also captured important episodic events including macrophyte sloughing that led to a pulse of respiration that represented 7% of the annual CO_2 gas efflux and cloudy periods that occurred every 7–18 days that dramatically decreased the pCO_2 through cooling.

Citation: Lynch, J. K., C. M. Beatty, M. P. Seidel, L. J. Jungst, and M. D. DeGrandpre (2010), Controls of riverine CO_2 over an annual cycle determined using direct, high temporal resolution pCO_2 measurements, *J. Geophys. Res.*, *115*, G03016, doi:10.1029/2009JG001132.

1. Introduction

[2] Rivers redistribute total organic carbon and total dissolved inorganic carbon (DIC) between the atmosphere and the terrestrial and oceanic systems [*Devol et al.*, 1995; *Richey*, 2004; *Richey et al.*, 2002; *Wachniew*, 2006] and are recognized as important components of the global carbon cycle [*Cole et al.*, 2007]. Inorganic carbon is a large pool of riverine carbon that is connected to organic carbon through primary production and respiration. Dissolved inorganic carbon also exchanges with the atmosphere when CO_2(aq), usually expressed as the pCO_2, is not in equilibrium with the atmosphere. Riverine pCO_2 cycles reveal internal riverine carbon dynamics and external processes of the surrounding terrestrial ecosystem [*Jones et al.*, 2003]. Measurements of pCO_2 and DIC and other inorganic carbon parameters such as pH can provide quantitative estimates of biological productivity, community respiration, gas exchange, calcification, and export of inorganic carbon. Moreover, the CO_2 buffer system, primarily in the form of HCO_3^-, typically controls river pH along with chemical speciation, solubility, and kinetics. In most cases, if riverine CO_2 cycles are well understood, pH regulation is also well understood.

[3] Previous research has characterized riverine pCO_2 cycles during both short-term and long-term periods. These studies have found that the majority of riverine ecosystems are sources of CO_2 to the atmosphere [*Barth et al.*, 2003; *Barth and Veizer*, 1999; *Cole and Caraco*, 2001; *Devol et al.*, 1995; *Jones et al.*, 2003; *Pinol and Avila*, 1992; *Richey*, 2004; *Richey et al.*, 2002; *Striegl et al.*, 2007; *Wachniew*, 2006]. It is generally thought that CO_2 supersaturation results from the respiration of terrestrial organic carbon and input of CO_2-rich groundwater [*Cole and Caraco*, 2001; *Jones et al.*, 2003; *Richey*, 2004; *Richey et al.*, 2002; *Worrall and Lancaster*, 2005]. Rivers very efficiently remineralize terrestrial carbon [*Richey*, 2004], and because rivers have high gas exchange rates and little or no organic carbon storage, much of the CO_2 is released to

[1]Department of Chemistry, University of Montana, Missoula, Montana, USA.

0148-0227/10/2009JG001132

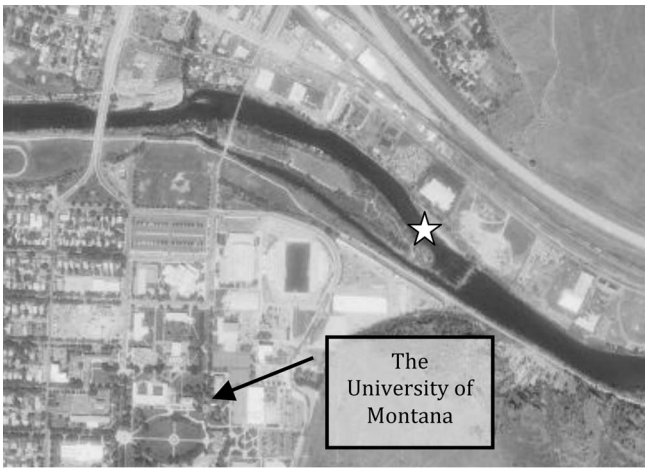

Figure 1. Location of the sensor deployment site (white star) in the Clark Fork River near the University of Montana campus. Image provided courtesy of USGS.

the atmosphere. Total riverine efflux to the atmosphere and riverine export of organic and inorganic carbon to the oceans are estimated to be a large fraction of the global terrestrial net ecosystem production (NEP) [*Cole et al.*, 2007]. It is possible that the existing estimates of carbon accumulation by the terrestrial ecosystem are in fact overestimates because they have not taken into account waterborne fluxes [*Hope et al.*, 2001; *Richey et al.*, 2002]. Therefore, understanding the mechanisms that control riverine carbon dynamics is an important objective.

[4] A lack of high-resolution pCO_2 data has made it difficult to characterize and model CO_2 cycling in rivers and to determine the role of short-term processes on long-term carbon fluxes. Moreover, few studies have used direct measurements of pCO_2 in riverine systems [*Cole and Caraco*, 2001]. Much of the riverine pCO_2 data reported in the literature were calculated from more commonly measured parameters including pH, total alkalinity (A_T), or DIC [*Barth et al.*, 2003; *Devol et al.*, 1995; *Jones et al.*, 2003; *Wachniew*, 2006]. If two of these parameters are measured along with the water temperature, pCO_2 can be calculated, but errors in pCO_2 can be large even for relatively small errors in the other parameters [*Herczeg and Hesslein*, 1984]. Consequently, high-quality measurements of pCO_2 and DIC with dense temporal coverage that extend for long periods should give a more accurate understanding of inorganic carbon fluxes in fluvial systems.

[5] We undertook a multiyear study using autonomous CO_2 sensors to accurately establish the annual range of pCO_2 variability, quantify fluxes, and elucidate the processes that control riverine CO_2. A total of 23,941 pCO_2 measurements were made from 2002 to 2006 in the Clark Fork River (CFR), Montana, USA, comprising one of the longest duration, high temporal resolution riverine pCO_2 data sets ever obtained. In this paper, we present the observed CO_2 cycles on both diel and seasonal time scales, use additional physical and chemical measurements as well as modeling to determine the processes that control riverine CO_2 cycling, quantify the gas exchange and biological fluxes and compare them to those found in previous studies, and evaluate the extent to which short-term episodic events control riverine pCO_2 and inorganic carbon.

2. Methods

2.1. Site Description

[6] The 563 km CFR drains a total area of 67,340 km^2 from its headwaters near Butte, Montana, to its terminus in Lake Pend Orielle, Idaho [*Patrick*, 1995]. The CFR is a fourth-order, high-gradient, cobble-bed, open-canopied, alkaline river. The study site was located in Missoula, Montana, at an elevation of ~972 m near the University of Montana campus (Figure 1). The mean peak and base flows at the study site are 250 and 40 $m^3\ s^{-1}$, respectively, from a watershed area of ~15,500 km^2. At the time of the study, the Milltown Dam and Reservoir were located ~5 km upstream. The dam has since been removed as part of a large-scale remediation of contaminated sediments in the Clark Fork watershed. During the study period, the Milltown Dam was not actively regulated and did not significantly alter the discharge except for occasional drawdowns for maintenance. The 5 km section of the CFR below the dam is a well-known losing reach that replenishes the Missoula valley aquifer [*Gestring*, 1994]. The riparian area upstream from the study site is relatively unsettled in comparison to other large temperate rivers in the contiguous United States. Periphyton dominates the biomass over the study reach and is composed primarily of diatoms and filamentous green algae (e.g., *Cladophora*), although there are also species of blue-green algae [*Gestring*, 1994].

2.2. Measurements and Data Sources

[7] Field deployments spanned from May 2002 to June 2006. Sensors for pCO_2, depth, and temperature were deployed at various times throughout the period. All instruments were protected in a stainless steel mooring cage anchored to the riverbed. When possible, the instruments were deployed at a depth of ~0.5 m, completely submerging the instruments but still allowing easy access for data download and maintenance.

[8] Measurements of pCO_2 and temperature were made using a Submersible Autonomous Moored Instrument for CO_2 (SAMI-CO_2) [*DeGrandpre et al.*, 1995]. The SAMI measurement is based on the equilibration of dissolved CO_2 with a pH indicator contained within a gas-permeable membrane. The SAMIs were usually deployed with a submersible pump and protective flow cell to reduce fouling and sediment accumulation on the membrane. All measurements were made on a 30 min interval. We do not have the capability to measure pCO_2 on discrete samples; thus, for quality control purposes, pCO_2 was calculated from pH and A_T measured on samples. CO_2 calculations were made using a CO_2 equilibrium program, CO2SYS [*Lewis and Wallace*, 1998], modified using the Davies equation to account for ionic strength dependence of the equilibrium constants for water and carbonic acid [*Stumm and Morgan*, 1996]. Ionic strength was estimated by using a linear relationship between A_T and ionic strength [*Mickey*, 1998]. DIC ($= CO_2(aq) + H_2CO_3 + HCO_3^- + CO_3^{2-}$) was calculated using the in situ pCO_2, water temperature, and interpolated A_T from the grab samples. Previous data at the study site

showed little short-term A_T variability, and we therefore assumed that the interpolated data could be used. Samples for pH and A_T analyses were collected in 500 mL glass bottles with no headspace to minimize CO_2 exchange. Laboratory analyses were completed within a few hours of sample collection.

[9] pH was measured using the indicator-based method [*Byrne and Breland*, 1989] adapted for freshwater [*French et al.*, 2002; *Yao and Byrne*, 2001; *Yuan and DeGrandpre*, 2008]. The pH accuracy and precision are estimated to be ~0.008 and ±0.002, respectively, at the buffer intensity typical of the CFR [*Yuan and DeGrandpre*, 2008]. This method was selected over potentiometric glass pH electrode methods because of the well-known electrode drift and junction potential errors that occur in low-ionic strength samples. These errors often lead to low pH values, which result in a calculated pCO_2 that is too high [*Cole and Caraco*, 2001; *Raymond et al.*, 1997]. A_T was measured using an automated potentiometric Gran titration. On the basis of replicate analyses of standards, A_T accuracy and precision are ~±5 μmol kg^{-1}.

[10] The average offset between the in situ pCO_2 and the pCO_2 calculated from pH and A_T was −2 ± 23 μatm (n = 15). Possible sources of error include pH or A_T measurement error, instrument fouling, or error in the SAMI-CO_2 calibration. There is no evidence of consistent systematic offsets, which could arise from errors in the instrument calibration or equilibrium constant model.

[11] Additional physical data were gathered from a number of sources to aid in the analysis of the pCO_2 data. River discharge measurements were obtained ~3.5 km upstream of the deployment site from U. S. Geological Survey (USGS) gauging station 12340500. Photosynthetically active radiation (PAR) data were obtained from the National Center for Environmental Prediction provided by the National Oceanic Atmospheric Administration (NOAA) Cooperative Institute for Research in Environmental Sciences Climate Diagnostics Center. The NOAA National Weather Service wind speed, air temperature, and precipitation were obtained from a weather station ~12 km from the deployment site. All of these data were compiled for the same time periods used in the CO_2 data set described below.

[12] A value of 380 ppm was assumed for atmospheric CO_2 mole fraction for clean air. At the local barometric pressure (0.89 atm), the resulting atmospheric pCO_2 (pCO_{2air}) is 338 μatm. Local atmospheric pCO_2 measurements during a 20 day period in September 2000 revealed diel variations from 332 to 372 μatm, with a mean of 345 ± 14 μatm [*Reynolds*, 2001], corrected for the increase in atmospheric CO_2 since that time. Because the mean is close to the clean marine air CO_2 level (338 μatm, referenced to 2006 values at Niwot Ridge from http://cdiac.ornl.gov) and pCO_{2air} is unknown during other periods, we used 338 μatm for pCO_{2air} in calculations and plots.

2.3. Data Analysis

[13] Previous studies have shown that riverine pCO_2 variability is strongly influenced by stream discharge, temperature change, gas exchange with the atmosphere, groundwater accrual, and river metabolism [e.g., *Devol et al.*, 1995; *Finlay*, 2003]. The mass balance accounting for these processes, in terms of DIC, is [*Thyssen and Kelly*, 1985]

$$H \quad \frac{\mathrm{dDIC}}{\mathrm{d}t} = F_{\mathrm{GAS}} \quad \mathrm{NEP} + A + C, \tag{1}$$

where H is the river depth, dDIC/dt is the rate of change of DIC, F_{GAS} is the flux of CO_2 between air and water, NEP is net ecosystem production (gross primary production - ecosystem respiration), A is the accrual of groundwater, and C is calcium carbonate formation or dissolution.

[14] Using the single-station approach of *Odum* [1956], NEP can be determined from the change in DIC per unit time (dt, where dt is the measurement interval) less the air-water flux. We assume that the mean NEP during a 24 h period is only affected by short-term processes and that A and C are negligible during the diel cycle. Significant errors in O_2-based measurements of NEP can occur from groundwater accrual [*McCutchan et al.*, 2002]. Processes such as evapotranspiration can lead to diel changes in groundwater flow; however, no diel changes in discharge were evident in the long-term 15 min resolution USGS record. Seasonally, however, groundwater is an important contributor to the CO_2 budget, as discussed below.

[15] We estimated F_{GAS} for the CFR using

$$F_{\mathrm{GAS}} = K_{\mathrm{C}} \quad K_{\mathrm{H}} \quad \Delta pCO_2, \tag{2}$$

where K_C is the gas transfer velocity for CO_2, K_H is Henry's constant representing the solubility of CO_2 in water [*Weiss*, 1974], and ΔpCO_2 is the difference between pCO_{2air} (338 μatm) and pCO_{2water}. K_C was estimated using a relationship with K_O, where $K_C = K_O \times 0.915$ and K_O is the gas transfer coefficient for oxygen [*Thyssen and Kelly*, 1985]. K_O is found by first calculating the reaeration coefficient K_2, where $K_2 = K_O/H$ [*Moog and Jirka*, 1998] and H is water column height (in m). K_2 is typically calculated using predictive equations that use stream hydraulics [*Moog and Jirka*, 1998]. Because of the wide range of riverine conditions that control K_2, a single equation to calculate the reaeration coefficient for every stream does not exist. A comparison of gas transfer velocity studies in rivers has shown a general lack of agreement both among the studies and between physically based predictive models [*Raymond and Cole*, 2001]. Therefore, to get an idea of the range that different methods estimate, two different equations were used to calculate K_2 for the CFR. These two equations were chosen because the range of physical and hydraulic parameters that they were derived from match those of the CFR. These equations are

$$K_2\left(\mathrm{d}^{-1}\right) = 596 \quad (VS)^{0.528} \quad Q^{-0.136} \text{ [Melching and Flores, 1999] and} \tag{3}$$

$$K_2\left(\mathrm{d}^{-1}\right) = 1740 \quad V^{0.46} \quad S^{0.79} \quad H^{0.74} \text{ [Moog and Jirka, 1998]}, \tag{4}$$

where V is stream velocity (in m s^{-1}), S is water-surface slope (in m m^{-1}), Q is discharge (in m^3 s^{-1}), and H is water column height (in m). V was found by dividing the reported Q by the CFR width and depth. The width of the CFR was measured at both low- and high-flow periods using a handheld Global Positioning System receiver.

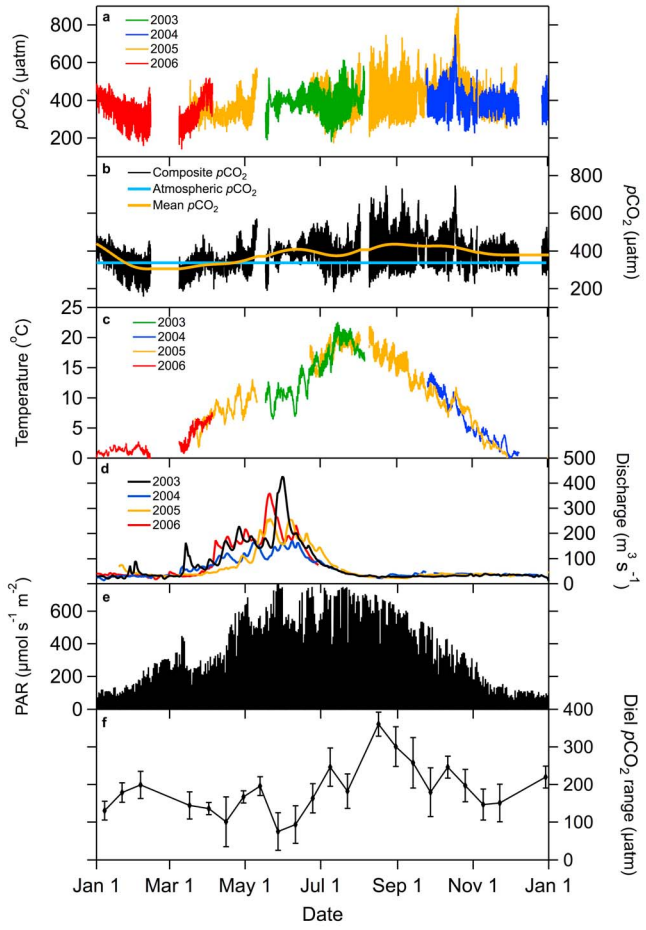

Figure 2. (a) pCO_2 measured by the SAMI-CO_2 from 2002 to 2006. (b) Composite pCO_2 data with mean riverine pCO_2 (yellow line) and atmospheric pCO_2 (blue line). Mean pCO_2 was calculated using a 4 week low-pass filter. (c) Temperature data from 2002 to 2006. (d) Discharge data from 2003 to 2006. (e) PAR data from 2005 from the National Center for Environmental Prediction. (f) Diel pCO_2 range calculated by averaging the difference of the daily maximum and minimum pCO_2 values during 2 week periods.

Depth was measured using a measuring stick at multiple points along the cross section of the river at the deployment site. The average depth across the study section measured using this technique was found to be nearly the same as the USGS gauge height. Daily USGS gauge measurements were then interpolated to 0.5 h intervals to correspond to the pCO_2 measurement interval. Mean depth at the deployment site for a typical year was 0.52 ± 0.18 m. S was found to be 0.0014 m m^{-1} using topographical floodplain maps. The CFR rarely completely freezes over, and if so, only for short periods; therefore, gas exchange estimates were made for the entire year.

[16] The method developed by *Takahashi et al.* [2002] for marine studies was used to evaluate the effects of heating and cooling on pCO_2. Changes from the mean pCO_2 (pCO_{2mean} = 380 μatm) were calculated relative to the annual mean temperature (T_{mean} = 9.0°C) at the deployment site, using

$$pCO_2 \text{ at } T_{obs} = pCO_{2mean} \exp[0.0384 (T_{obs} - T_{mean}), \quad (5)$$

where T_{obs} is the measured in situ temperature, the coefficient 0.0384°C^{-1} is the temperature effect on pCO_2 for isochemical freshwater determined using CO2SYS [*Lewis and Wallace*, 1998], and pCO_2 at T_{obs} represents the pCO_2 value that would be expected if a parcel of water with a mean pCO_2 value of 380 μatm is subjected only to changes in temperature, no biological or other effects, in isochemical water. pCO_2 increases with increasing temperature, as shown in equation (5) because of the decreased solubility of CO_2 (pCO_2 = $CO_2(aq)/K_H$, where K_H is the Henry's law of solubility) and the increase in CO_2(aq) from the $H^+ + HCO_3^-$ equilibrium.

3. Results

3.1. Data Overview

[17] The 23,941 pCO_2 measurements gathered from 2002 to 2006 are shown in Figure 2a. The very noisy appearance of the data originates from the large diel cycle. Collecting a full year of continuous pCO_2 data proved to be very challenging. Adverse conditions that are unique to a riverine system, including encasement of the instrument in bottom ice, extensive sedimentation on the sensor membrane, and inaccessibility during the ~2 month spring high-discharge period led to data gaps. To assemble a yearlong pCO_2 data set, the data were compiled into a composite year, choosing the longest continuous records to facilitate data processing rather than averaging overlapping periods. Averaging would be appropriate for seasonal means, but an interannual average of short-term variability would not be readily interpretable. The resulting composite data set is composed of 14,818 measurements covering ~309 days (Figure 2b). The interannual consistency of the pCO_2 and temperature gave us confidence in using the separate years of data to construct the composite pCO_2 data set and analyze it for trends. Detailed comparisons of interannual variability are outside the scope of this study.

3.2. Major Features

[18] The pCO_2 ranged from ~100 to 900 μatm, with a mean pCO_2 of 380 ± 80 μatm (Figure 2b). Water temperature ranged from 0°C to 23°C, and the mean annual temperature was 9.0°C (Figure 2c). Varying spring weather and snowpack led to interannual differences in the timing and magnitude of maximum flow (Figure 2d). PAR increased rapidly in the spring, but long periods of clouds, characteristic of the region, persisted through early summer (Figure 2e). The water temperature typically responded to this variability by briefly plateauing in the spring and then rapidly increasing during the extended sunny periods in July (Figure 2c).

[19] The 4 week-averaged (mean) pCO_2 ranged from 310 to 440 μatm and was above atmospheric levels (338 μatm) from midspring to midwinter, only dropping below saturation between February and May (Figure 2b). The period of undersaturation corresponds not only to the coldest temperatures but also to a period of increasing PAR. Highest

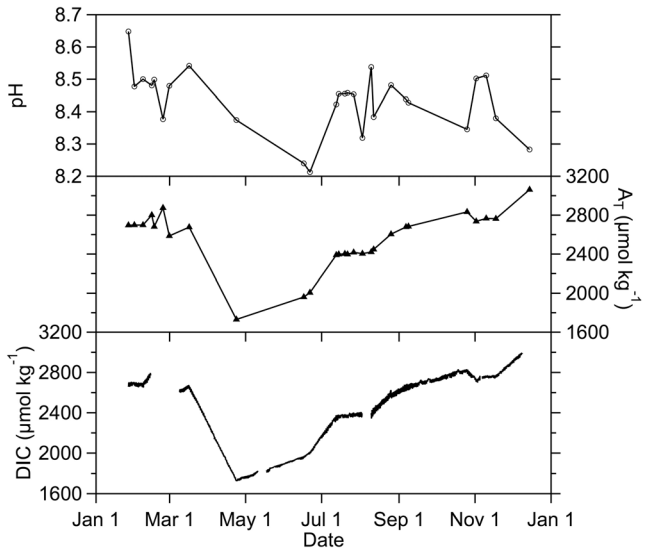

Figure 3. Plots of spectrophotometric (top) pH and (middle) A_T measured on grab samples and (bottom) calculated DIC. A_T and pH measurements were made from the summer of 2005 to the spring of 2006.

mean CO_2 supersaturation occurred in late summer during the low-flow period but after the peak in water temperature.

[20] In the CFR, highly regular, large-amplitude diel cycles dominated the pCO_2 variability. The pCO_2 changed by as much as 460 μatm during a diel cycle. The diel pCO_2 seasonal trend was calculated by averaging the difference of the daily maximum and minimum pCO_2 values during 2 week periods. The averaged diel pCO_2 amplitude ranged from 75 to 360 μatm (Figure 2f), and during January and February, this approached 200 μatm even when water temperature and light were near their lowest levels.

[21] All of the additional measured and calculated CO_2 parameters (pH, A_T, and DIC) had large seasonal variability (Figure 3). The measured pH varied from a minimum of 8.21 in July to a maximum of 8.65 in January. During the summer, the high temporal resolution pH, calculated from pCO_2 and interpolated A_T, changed by as much as 0.5 during a diel cycle (not shown). A_T ranged from a spring minimum of 1640 μmol kg^{-1} to a winter maximum of 3060 μmol kg^{-1}. The calculated DIC mirrored the A_T, with a minimum of 1740 μmol kg^{-1} during spring and a maximum of 3090 μmol kg^{-1} during early winter. In contrast to pCO_2, the diel DIC variability, seen as the thicker portions of the DIC time series curve, is much smaller than the seasonal DIC range. Analysis of the sources of diel to seasonal variability is presented in section 4.

4. Discussion

4.1. Air-Water Flux

[22] The pCO_2 levels, consistently above atmospheric saturation but higher in summer and lower in winter, are similar to those observed in the much larger Hudson River [*Raymond et al.*, 1997] and other temperate streams [e.g., *Worrall et al.*, 2005; *Finlay*, 2003]. Riverine systems, including tropical rivers, typically have a strong seasonal CO_2 cycle [*Devol et al.*, 1995; *Richey et al.*, 2002]. Also, like other rivers [*Cole and Caraco*, 2001], the CFR is a net source of CO_2 to the atmosphere. The net supersaturation in the CFR yields a total flux of 7.1–4.7 mol C m^{-2} yr^{-1} based on the *Melching and Flores* [1999] and *Moog and Jirka* [1998] gas transfer rates, respectively (equations (2)-(4); mean = 5.9 mol C m^{-2} yr^{-1}). The gas transfer rate of *Moog and Jirka* [1998] is significantly lower than that of *Melching and Flores* [1999] during low-flow periods. Additional uncertainty arises from the atmospheric value, which is assumed constant but is influenced significantly by local terrestrial fluxes and interannual variability and is likely underestimated at this site. The flux is sensitive to this value; that is, increasing the mean atmospheric CO_2 level by 10 ppm decreases the net efflux by 25%. The uncertainties are particularly important in estimating NEP, as discussed below.

[23] The CFR efflux is much less than the 34 mol C m^{-2} yr^{-1} average CO_2 efflux estimated for 47 major rivers around the world [*Cole and Caraco*, 2001]. The mean pCO_2 of the 47 rivers was 3230 μatm, more than 8 times the mean pCO_2 measured for the CFR (380 μatm). Many of these rivers, such as the Mississippi, Hudson, Amazon, and Niger, are also much larger, have more allochthonous organic carbon input, and are considerably warmer. A study of pCO_2 levels in rivers across the contiguous United States showed that the northwest and Rocky Mountain regions have lower pCO_2 levels (similar to those of the CFR) than those in other regions as a consequence of lower leaf litter production and soil organic matter decomposition [*Jones et al.*, 2003]. It is also possible that the data sets used for the 47 rivers were biased because of undersampling or pH systematic errors, as discussed earlier. If samples were gathered in the morning, for example, the resulting mean CFR pCO_2 could be hundreds of microatmospheres higher than the mean diel level. Large (>300 μatm) diel pCO_2 changes have also been observed in large rivers, but these changes were considered negligible relative to the overall supersaturation [*Raymond et al.*, 1997]. However, when calculating pCO_2 from electrode-based pH, *Herczeg and Hesslein* [1984] found a twofold positive bias in pCO_2 supersaturation because of the systematically low-electrode pH.

4.2. Controls of Diel pCO_2 Variability

4.2.1. General Trends

[24] Unlike many other aquatic ecosystems, the river diel amplitude was considerably larger than the range of seasonal variability represented by the 4 week-averaged data (Figure 2b). The largest diel cycles occurred during times of low discharge, high temperature, and PAR, whereas the minimum diel pCO_2 range occurred at times of highest discharge (Figure 2). The diel pCO_2 range was correlated with 2 week-averaged discharge (Q; $r^2 = 0.32$, $p < 0.01$; Figure 4a) but was not correlated with PAR or temperature (not shown). It is likely that the decrease in the diel amplitude with discharge originates from decreased biological production in the deep and turbid runoff water in addition to the scouring of biofilms that occurs during floods [*Uehlinger*, 2006]. Normalizing PAR to Q results in a better correlation ($r^2 = 0.51$, $p < 0.001$; Figure 4b) than PAR alone because it separates the low-PAR periods (e.g., winter), when the diel range was still quite large, from the higher-PAR high-Q periods (late spring) when the diel range was small (Figure 2). These seasonal forcings, Q and PAR,

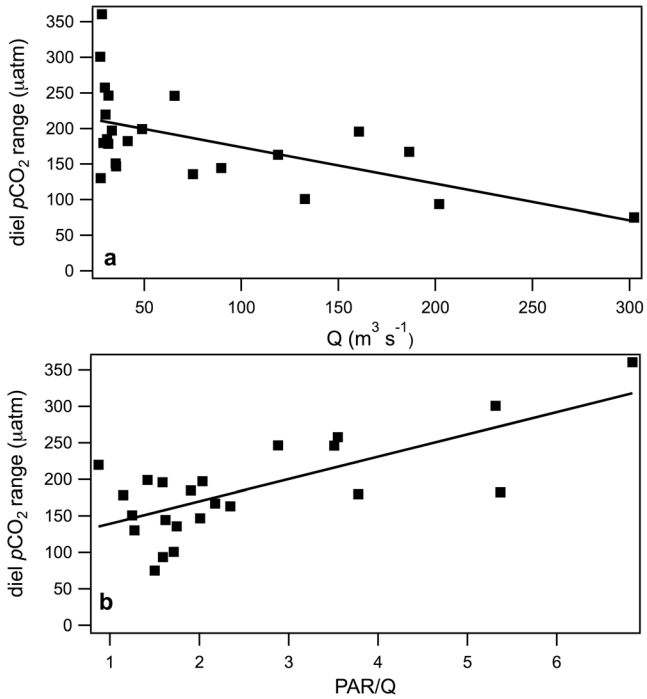

Figure 4. The diel pCO_2 range (Figure 2f) relationship with (a) discharge (Q; $r^2 = 0.32$, $p < 0.01$) and (*b*) PAR/Q ($r^2 = 0.51$, $p < 0.001$; see text for more details).

regulate the underlying processes of heating/cooling and ecosystem production, which directly affect the diel pCO_2 range [*Parker et al.*, 2005] as discussed in more detail below. Also, at higher Q, dilution reduces water column changes in pCO_2 for a given level of biological activity.

4.2.2. Diel Temperature

[25] Diel heating and cooling significantly contribute to the observed diel cycle of pCO_2. In the CFR, the observed diel temperature increase was as large as 4°C, which would increase pCO_2 by ~60 μatm during the day (equation (5)) because of the decreased solubility and the increase in CO_2(aq). Even during the winter, daytime heating could be as large as 0.5°C. The increase in pCO_2 expected from heating, however, was masked by the biological uptake of CO_2 for all seasons, as discussed in more detail below.

4.2.3. Diel Gas Exchange

[26] Large air-water CO_2 gradients, small depths, and high turbulence characteristic of rivers make air-water gas exchange a potential contributor to short-term pCO_2 variability. At the peak air-water flux (0.12 mol m^{-2} d^{-1}), DIC decreased at a rate of 5 μmol kg^{-1} h^{-1} because of the gas exchange. These large changes in DIC could alter the pCO_2 (and pH) during diel periods. To calculate this effect, F_{GAS} (equations (2)-(4)) was added back into the DIC, and the pCO_2 and pH were recalculated using CO2SYS and the interpolated A_T. The pCO_2 with gas exchange effects removed is shown for a high flux period in Figure 5 (pH not shown). The air-water exchange significantly decreases the nighttime pCO_2 maximum. In August, when pCO_2 supersaturation was highest, the nighttime pCO_2 amplitude was suppressed by more than 50 μatm based on the larger *Melching and Flores* [1999] flux. This release of CO_2 also altered the diel pH cycle by ~0.04 pH units. These are very large effects relative to other aquatic ecosystems where wind-driven gas exchange rates are low and changes in DIC are integrated over a large mixed layer depth [*DeGrandpre et al.*, 2004]. These results reinforce the general thought that CO_2 gas exchange must be measured or calculated for accurate diel CO_2 mass balances in rivers and streams [e.g., *Thyssen and Kelly*, 1985].

4.2.4. Diel Net Ecosystem Production

[27] NEP is one of the most important influences on riverine carbon cycles [*Barth and Veizer*, 1999; *Finlay*, 2003; *Guasch et al.*, 1998]. As discussed above and shown in equation (1), the 24 h (diel) NEP can be estimated by correcting the DIC rates of change for gas exchange. The single-station approach used here assumes homogeneous upstream conditions, and this will generate errors in NEP if this is not the case. At this location, upstream water was delayed ~10 h by the reservoir, creating a double peak or shoulder in the diel pCO_2 data (Figures 5 and 6). When the residence time decreased because of the drawdown of the reservoir for dam maintenance, the double peak disappeared. We showed in a previous short-term upstream-downstream study that these features could be eliminated by subtracting the upstream from the downstream pCO_2 [*Reynolds*, 2001]. In this single-point measurement, the reservoir could potentially alter the NEP, but we found that it had no effect on the 24 h mean NEP. The nighttime respiration, however, is sometimes biased, because CO_2 can decrease at night owing to the delayed reservoir peak; therefore, gross primary production, which requires nighttime estimates of ecosystem respiration, could not be accurately calculated.

[28] NEP is usually comparable to the gas flux because, during a 24 h period, the net DIC change is typically near zero, and therefore, NEP has to compensate for any net loss or gain of CO_2 due to the air-water exchange. There were some periods, however, with large net diel changes in pCO_2 and DIC (e.g., Figure 6, top). These events show up as strong negative peaks in NEP (Figure 7) and correlate with rain events ($r^2 = 0.152$, $p < 0.01$; Figure 8). Rain can increase pCO_2 and DIC through the CO_2 and organic carbon-enriched runoff [e.g., *Manny and Wetzel*, 1973] or by

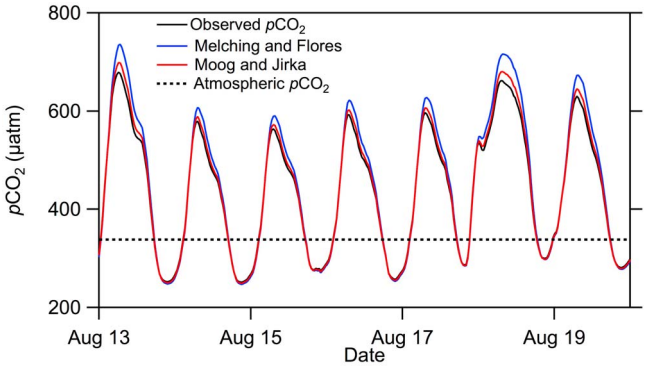

Figure 5. Diel pCO_2 with the effects of gas exchange removed. The observed pCO_2 (black curve), pCO_2 with the gas exchange estimated using the equation from *Moog and Jirka* [1998] (red curve) and *Melching and Flores* [1999] (blue curve) and atmospheric pCO_2 (dotted line) are shown.

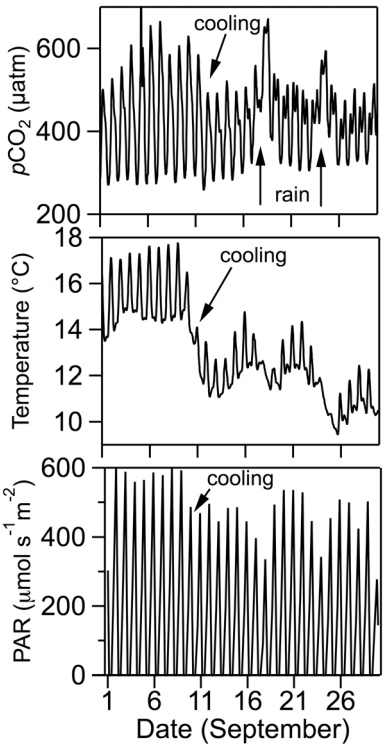

Figure 6. (top) An example of short-term events that altered the pCO_2 diel amplitude and baseline. In early September 2005, a cold front came through, as indicated by the decrease in (middle) temperature and (bottom) PAR, which dramatically decreased the pCO_2. Other rain events also drove large changes in pCO_2 (see text for more discussion).

scouring biomass that disproportionately decreases photosynthesis over respiration [*Uehlinger*, 2006]. Because the pCO_2 rapidly returned to its baseline value (Figure 6, top) and the discharge did not typically increase dramatically during rain events, scouring is an unlikely cause. More plausibly, the CO_2 pulses are from CO_2 in runoff. On the basis of the evaluation of data such as those shown in

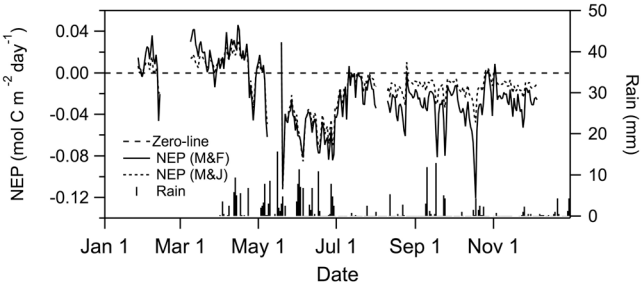

Figure 7. Net ecosystem production calculated using the open water method of *Odum* [1956] (equation (1)). The large peaks during spring-fall correlated with rain events (also shown; Figure 8). The influence of rain events was removed from the calculation of the mean NEP (see text). M&F, *Melching and Flores* [1999] gas flux calculation; M&J, *Moog and Jirka* [1998] gas flux calculation. The zero (dashed) line marks the boundary between net respiration (NEP < 0) and net production (NEP > 0).

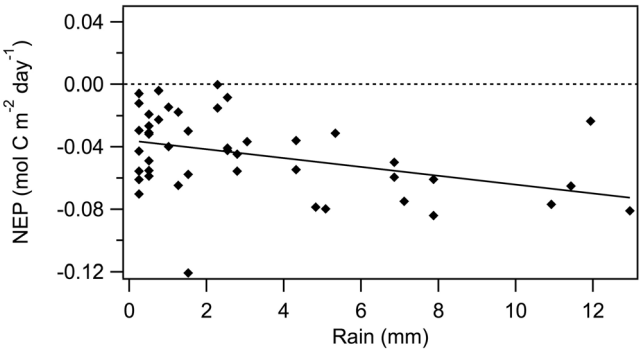

Figure 8. Relationship between NEP and rain from June to November ($r^2 = 0.152$, $p < 0.01$). The best correlation was found with a 1 day phase shift between the two data sets. The correlation broke down if spring rain events were included.

Figure 6, the CO_2 pulse lagged rain events, and it was found that NEP and rain were not well correlated unless the data were shifted by 1 day (the correlation shown in Figure 8). If spring rain data are included in Figure 8, the positive NEP during this time degrades the correlation. By removing the rain events, the mean annual NEP decreases by ~21% to −16.5 and −11 mmol m^{-2} d^{-1} for the gas exchange rates of *Moog and Jirka* and *Melching and Flores*, respectively (mean = −13.8 ± 3 mmol m^{-2} d^{-1}). The seasonal trends in NEP are discussed below.

4.3. Other Short-Term Processes

[29] Whereas NEP typically dominated the diel pCO_2 variability, episodic cooling and heating events also created large changes in pCO_2. For example, the mean pCO_2 decreased by ~100 μatm during a cloudy period in early September 2005. This drop in pCO_2 is about what would be expected from the observed ~5°C decrease in temperature (Figure 6). On the basis of a visual analysis of the temperature data, these cool, cloudy periods occurred every 7–18 days. There is no correlation between temperature and pCO_2 for the full data set (see below); however, Fourier analysis of the pCO_2 data found a peak at period of 11 days (not shown), likely corresponding to these regional weather events.

[30] The high temporal resolution pCO_2 data set also captured other unusual episodic events. In mid-October of both 2004 and 2005, there was a sudden spike in the pCO_2 (Figures 2a and 6). The large CO_2 increase was most likely due to the die-off and subsequent decomposition of the macrophytic periphyton community (*Cladophora glomerata*) that typically occurs in the fall (V. Watson, University of Montana, personal communication, 2007). This die-off may have been triggered as the water temperature dropped (Figure 2c). *Cladophora* growth is known to be regulated by temperature [*Dodds*, 1991] and optimal at higher temperatures [*Lester et al.*, 1988]. A study using continuous O_2 data observed biofilm sloughing that dramatically altered both net production and respiration [*Uehlinger*, 2006]. In the CFR, the macrophyte die-off led to a large pulse of respiration (Figure 7); this single event changed the annual air-water gas flux by 7% using the larger flux estimate of *Melching and Flores* [1999].

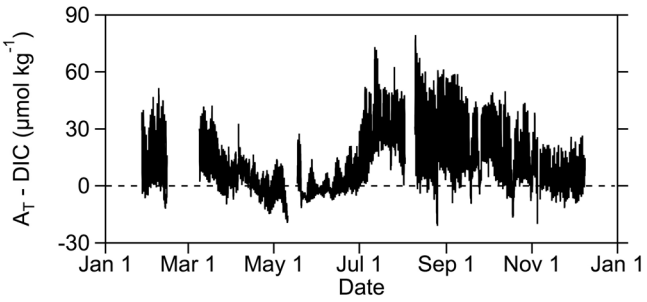

Figure 9. Difference between interpolated A_T and DIC showing the seasonal contributions from groundwater input relative to net NEP and the large diel DIC cycle (see text for more discussion).

4.4. Controls of Seasonal pCO_2 and Inorganic Carbon

4.4.1. General Trends

[31] The seasonal pH, A_T, and DIC patterns (Figure 3) follow discharge, with the lowest values corresponding to high discharge in the spring and highest values occurring during the summer through winter base flow periods. The correlation of DIC with Q is much better than pCO_2 with Q, r^2 = 0.76 and 0.01, respectively (not shown). The large short-term pCO_2 variability is dominated by temperature and NEP, as discussed above, and masks any seasonal relationship of pCO_2 with Q. The seasonal DIC variability, in contrast, is quite large relative to the diel cycles (the fuzzy appearance of the calculated DIC data in Figure 3). Discharge has been shown to control the seasonal magnitude of inorganic carbon in a wide range of lotic systems, e.g., the Vistula in Poland, forested Mediterranean catchments in Spain, a braided river in Scotland, and the Amazon [*Devol et al.*, 1995; *Pinol and Avila*, 1992; *Rodgers et al.*, 2004; *Wachniew*, 2006]. Although the contribution to this correlation from surface or groundwater varies from river to river, the CFR relationship is likely derived from increased groundwater (high DIC and A_T) at base flows relative to surface runoff from spring snowmelt.

[32] The difference between the interpolated A_T and DIC during the annual cycle can be used to remove the discharge-driven seasonal pattern and provide insights into other sources of variability (Figure 9). A_T can increase relative to DIC via groundwater input of carbonate minerals, in-river dissolution of $CaCO_3$, and NEP. Although $CaCO_3$ formation and dissolution occurs seasonally (J. Moore, personal communication, 2009), it is assumed to negligibly affect the water column. Relative to DIC, A_T is only weakly affected by photosynthesis, and we assumed that this could be ignored. A_T-DIC therefore represents the balance between groundwater input of CO_3^{2-} and DIC changes that do not significantly affect A_T, i.e., NEP, atmospheric exchange, and terrestrial and groundwater input of CO_2–rich water. As shown in Figure 9, the difference varied seasonally with the largest A_T surplus during the more productive summer (July–August), high CO_2 supersaturation, and low-flow period. A_T increased relative to DIC as the proportion of surface to groundwater decreased, net respiration was low (Figure 7), and CO_2 loss to the atmosphere was high. DIC consistently exceeded A_T only during peak runoff (May–June) when DIC increased from terrestrial carbon input and high net respiration (Figure 7). These observations are consistent with the discussions of NEP presented above. Figure 9 also more effectively shows the large diel DIC variability driven by NEP. DIC changes ranged from ~5 μmol kg^{-1} d^{-1} during spring runoff to 80 μmol kg^{-1} d^{-1} during August.

4.4.2. Seasonal NEP

[33] Ecosystem respiration typically exceeded photosynthesis during the year (Figure 7). The CFR was autotrophic during most of the winter and early spring but became heterotrophic during spring runoff and remained that way through the rest of the year. These two metabolic phases are likely driven by water temperature and organic carbon inputs as suggested by other studies [e.g., *Uehlinger*, 2006; *Worrall et al.*, 2005]. During the cold months, water temperature suppresses microbial decomposition and low runoff reduces allochthonous organic carbon input, while, at the same time, there is sufficient light to support primary production. As the water warms, rates of respiration increase and spring runoff and precipitation add organic carbon (and dissolved CO_2). The highest sustained rates of heterotrophy occurred from May to July, corresponding to a period of high discharge, warmer water and highest annual gas transfer rates. Many of the large changes in Figure 7 are due to rain events, but there are other rapid short-term changes that cannot be explained or predicted, and there is no significant correlation between NEP (with the rain events removed) and PAR, Q, or temperature. The lack of measurements of biological substrates (particulate and dissolved organic carbon, nutrients, and biomass) and rates under different physical conditions (PAR and temperature) limits our interpretation to these qualitative descriptions.

[34] The mean NEP (−13.8 ± 3 mmol m^{-2} d^{-1}) for this semiarid mountain river is less than that reported for larger rivers such as the −20 to −40 mmol C m^{-2} d^{-1} estimated for the Hudson River on the U. S. east coast [*Cole and Caraco*, 2001]. Lotic gross primary production (GPP) has been found to be only weakly dependent on climate variables (e.g., temperature and precipitation) and nutrients but increases with increasing watershed area and discharge and decreasing canopy cover [*Lamberti and Steinman*, 1997]. The lower net heterotrophy in the CFR relative to larger rivers such as the Hudson River is consistent with *Lamberti and Steinman*'s [1997] findings that medium-sized streams with low canopy cover typically have the highest GPP.

4.4.3. Seasonal Temperature Effects

[35] Figure 10 shows that the seasonal cycle of heating and cooling contributed significantly to the seasonal pCO_2 range but less so to the diel amplitude (note the comparatively small range of short-term variability compared with the range of the measured pCO_2). The annual temperature increase from 0°C to 23°C increased the pCO_2 by ~300 μatm; however, pCO_2 does not correlate with temperature during the annual cycle (r^2 = 0.07). The observed pCO_2 range is larger (~500 μatm) and does not closely resemble the temperature-driven pCO_2 because it is masked and is counteracted by the diel NEP and other short-term changes along with seasonal discharge, as discussed above. In the winter, pCO_2 continued to trend downward, while the temperature remained at its seasonal minimum, and in July, the mean pCO_2 also began to decline while temperature increased.

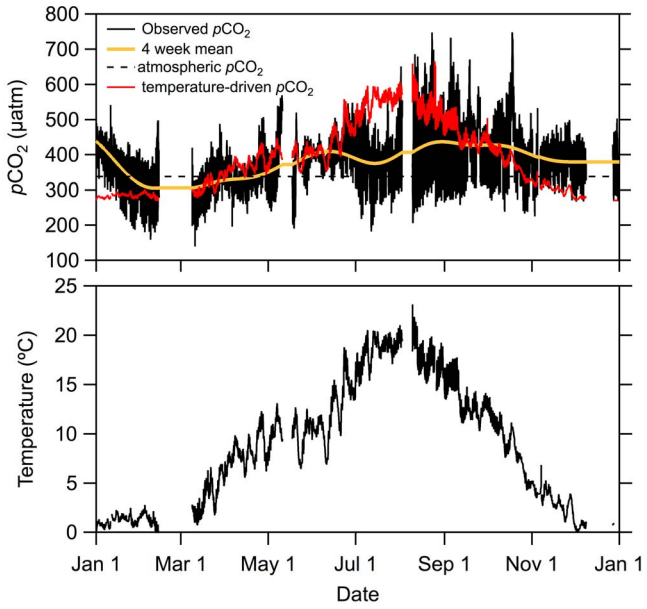

Figure 10. Thermodynamic (heating/cooling) effects on the annual pCO_2 cycle. (top) The black curve represents composite pCO_2 data from Figure 2b. The red line represents the pCO_2 cycle that would occur because of heating and cooling relative to the mean annual pCO_2 (380 μatm). The dashed line represents the atmospheric pCO_2 level, and the yellow line represents the monthly mean pCO_2 (Figure 2b). (bottom) One year composite plot of the temperature recorded in the CFR.

These periods correspond to base flow periods when primary production was high and terrestrial CO_2 and organic carbon inputs were minimal. The modulation of pCO_2 by the cold cloudy periods can also be seen more clearly in Figure 10, with the largest changes in spring through early summer. As discussed above, these changes are not clear in the measured pCO_2 because of the large diel cycle.

5. Conclusions

[36] The pCO_2 time series data presented here reveal the many different temporal scales of variability in a riverine system. Although it has long been known that rivers are some of the most productive aquatic ecosystems [*Odum*, 1956], the dominance of the diel CO_2 cycle in the annual variability has not been well documented because of the lack of long-term high temporal resolution data. Diel pCO_2 variability in this heterotrophic system proved to be predominantly controlled by NEP, although gas exchange and temperature were found to have significant contributions. Short-term precipitation and cooling due to a cloudy weather also dramatically altered the river pCO_2 for short periods. Seasonal pCO_2 variability was primarily controlled by heating/cooling, NEP, and discharge. The CFR loses CO_2 to the atmosphere for the majority of the year, with only a brief period of undersaturation in the winter, driven by net autotrophy and low rates of respiration.

[37] The river lost 5.9 mol C m^{-2} yr^{-1} to the atmosphere while producing 5.0 mol C m^{-2} yr^{-1} via net respiration. A total of 2.2×10^8 mol C m^{-2} yr^{-1} were exported downstream in the form of inorganic carbon, corresponding to a total load of 74×10^6 kg carbon yr^{-1}. The DIC yield or total DIC load divided by watershed area was 0.40 mol C m^{-2} yr^{-1}. The yield is comparable to that found for other rivers, including the similarly sized Icelandic rivers [*Gislason et al.*, 2009] and much larger Alaskan rivers [*Striegl et al.*, 2007].

[38] Continuous measurements can improve our knowledge of riverine biogeochemical cycling. However, we still lack the ability to make long-term predictions of stochastic variability in critical parameters such as pCO_2 (Figure 2) and NEP (Figure 7). With continued efforts such as those presented here and by expanding the suite of in situ measurements, we hope that models that accurately predict riverine carbon and biogeochemical fluxes can be developed.

[39] **Acknowledgments.** The authors thank Vicki Watson from the University of Montana, Ric Hauer from the University of Montana Flathead Lake Biological Station, and Stephen Lynch and Todd Martz both from the Scripps Institution of Oceanography for helpful discussions. This research was funded by the National Science Foundation (NSF EAR-0337460).

References

Barth, J. A. C., and J. Veizer (1999), Carbon cycle in St. Lawrence aquatic ecosystems at Cornwall (Ontario), Canada: Seasonal and spatial variations, *Chem. Geol.*, *159*, 107–128.

Barth, J. A. C., A. A. Cronin, J. Dunlop, and R. M. Kalin (2003), Influence of carbonates on the riverine carbon cycle in an anthropogenically dominated catchment basin: Evidence from major elements and stable carbon in the Lagan River (N. Ireland), *Chem. Geol.*, *200*, 203–216.

Byrne, R. H., and J. A. Breland (1989), High precision multiwavelength pH determinations in seawater using cresol red, *Deep-Sea Res.*, *36*, 803–810.

Cole, J. J., and N. F. Caraco (2001), Carbon in catchments: Connecting terrestrial carbon losses with aquatic metabolism, *Mar. Freshwater Res.*, *52*, 101–110.

Cole, J. J., et al. (2007), Plumbing the global carbon cycle: Integrating inland waters into the terrestrial carbon budget, *Ecosystems*, *10*, 171–184.

DeGrandpre, M. D., T. R. Hammar, S. P. Smith, and F. L. Sayles (1995), In situ measurements of seawater pCO_2, *Limnol. Oceanogr.*, *40*, 969–975.

DeGrandpre, M. D., R. Wanninkhof, W. R. McGillis, and P. G. Strutton (2004), A Lagrangian study of surface pCO_2 dynamics in the eastern equatorial Pacific Ocean, *J. Geophys. Res.*, *109*, C08S07, doi:10.1029/2003JC002089.

Devol, A. H., B. R. Forsberg, J. E. Richey, and T. P. Pimentel (1995), Seasonal variation in chemical distributions in the Amazon (Solimoes) River: A multiyear time series, *Global Biogeochem. Cycles*, *9*, 307–328.

Dodds, W. L. (1991), Factors associated with dominance of the filamentous green alga *Cladophora glomerata*, *Water Res.*, *25*, 1325–1332.

Finlay, J. C. (2003), Controls of streamwater dissolved inorganic carbon dynamics in a forested watershed, *Biogeochemistry*, *62*, 231–252.

French, C. R., J. J. Carr, E. M. Dougherty, L. A. K. Eidson, J. C. Reynolds, and M. D. DeGrandpre (2002), Spectrophotometric pH measurements of freshwater, *Anal. Chim. Acta*, *453*, 13–20.

Gestring, S. L. (1994), The interaction of the Clark Fork River and Hellgate Valley Aquifer near Milltown, Montana, M.S. thesis, Univ. of Montana, Missoula.

Gislason, S. R., et al. (2009), Direct evidence of the feedback between climate and weathering, *Earth Planet. Sci. Lett.*, *277*, 213–222.

Guasch, H., J. Armengol, E. Marti, and S. Sabater (1998), Diurnal variation in dissolved oxygen and carbon dioxide in two low-order streams, *Water Res.*, *32*, 1067–1074.

Herczeg, A. L., and R. H. Hesslein (1984), Determination of hydrogen ion concentration in softwater lakes using carbon dioxide equilibria, *Geochim. Cosmochim. Acta*, *48*, 837–845.

Hope, D., S. M. Palmer, M. F. Billet, and J. J. Dawson (2001), Carbon dioxide and methane evasion from a temperate peatland stream, *Limnol. Oceanogr.*, *46*, 847–857.

Jones, J. B., E. H. Stanley, and P. M. Mulholland (2003), Long-term decline in carbon dioxide supersaturation in rivers across the contiguous United States, *Geophys. Res. Lett.*, *30*(10), 1495, doi:10.1029/2003GL017056.

Lamberti, G. A., and A. D. Steinman (1997), A comparison of primary production in stream ecosystems, *J. North Am. Benthol. Soc.*, *16*, 95–103.

Lester, W. W., M. S. Adams, and A. M. Farmer (1988), Effects of light and temperature on photosynthesis of the nuisance alga *Cladophora glomerata* (L.) Kutz from Green Bay, Lake Michigan, *New Phytol.*, *109*, 53–58.

Lewis, E., and D. W. R. Wallace (1998), Program developed for CO_2 system calculations, ORNL/CDIAC-105. Carbon Dioxide Inf. Anal. Cent. (CDIAC), Oak Ridge Natl. Lab., Oak Ridge, Tenn.

Manny, B. A., and R. G. Wetzel (1973), Diurnal changes in dissolved organic and inorganic carbon and nitrogen in a hardwater stream, *Freshwater Biol.*, *3*, 31–43.

McCutchan, J. H., Jr., J. F. Saunders III, W. M. Lewis Jr., and M. G. Hayden (2002), Effects of groundwater flux on open-channel estimates of stream metabolism, *Limnol. Oceanogr.*, *47*, 321–324.

Melching, C. S., and H. E. Flores (1999), Reaeration equations derived from U. S. Geological Survey database, *J. Environ. Eng.*, *125*, 407–414.

Mickey, J. W. (1998), The effects of discharge variation on dissolved element concentrations through Milltown Reservoir, Montana, M.S. thesis, Univ. of Montana, Missoula.

Moog, D. B., and G. H. Jirka (1998), Analysis of reaeration equation using mean multiplicative error, *J. Environ. Eng.*, *124*, 104–110.

Odum, H. T. (1956). Primary production in flowing waters, *Limnol. Oceanogr.*, *1*, 102–117.

Parker, S. R., S. R. Poulson, C. H. Gammons, and M. D. DeGrandpre (2005), Biogeochemical controls on diel cycling of stable isotopes of dissolved O_2 and dissolved inorganic carbon in the Big Hole River, Montana, *Environ. Sci. Technol.*, *39*, 7134–7140.

Patrick, R. (1995), *Rivers of the United States*, John Wiley, New York.

Pinol, J., and A. Avila (1992), Streamwater pH, alkalinity, pCO_2 and discharge relationships in some forested Mediterranean catchments, *J. Hydrol.*, *131*, 205–225.

Raymond, P. A., and J. J. Cole (2001), Gas exchange in rivers and estuaries: Choosing a gas transfer velocity, *Estuaries*, *24*, 312–317.

Raymond, P. A., N. F. Caraco, and J. J. Cole (1997), CO_2 concentration and atmospheric flux in the Hudson River, *Estuaries*, *20*, 381–390.

Reynolds, J. C. (2001), Distributed in situ gas measurements for the analysis and modeling of biogeochemical changes in the Clark Fork River, M.S. thesis, Univ. of Montana, Missoula.

Richey, J. E. (2004), Pathways of atmospheric CO_2 through fluvial systems, in *The Global Carbon Cycle: Integrating Humans, Climate, and the Natural World*, edited by C. B. Field and M. R. Raupach, pp. 329–340, Island Press, Washington, DC.

Richey, J. E., J. M. Melack, A. K. Aufdenkampe, V. M. Ballester, and L. L. Hess (2002), Outgassing from Amazonian rivers and wetlands as a large tropical source of atmospheric CO_2, *Nature*, *416*, 617–620.

Rodgers, P., C. Soulsby, J. Petry, I. Malcolm, C. Gibbins, and S. Dunn (2004), Groundwater-surface water interactions in a braided river: A tracer based assessment, *Hydrol. Processes*, *18*, 1315–1332.

Striegl, R. G., M. M. Dornblaser, G. R. Aiken, K. P. Wickland, and P. A. Raymond (2007), Carbon export and cycling by the Yukon, Tanana, and Porcupine rivers, Alaska, 2001–2005, *Water Resour. Res.*, *43*, W02411, doi:10.1029/2006WR005201.

Stumm, W., and J. J. Morgan (1996), *Aquatic Chemistry: Chemical Equilibria and Rates in Natural Waters*, 3rd ed., John Wiley, New York.

Takahashi, T., et al. (2002), Global sea-air CO_2 flux based on climatological surface ocean pCO_2 and seasonal biological and temperature effects, *Deep-Sea Res., Part II*, *49*, 1601–1622.

Thyssen, N., and M. G. Kelly (1985), Water-air exchange of carbon dioxide and oxygen in a river: Measurement and comparison of rates, *Arch. Hydrobiol.*, *105*, 219–228.

Uehlinger, U. (2006), Annual cycle and inter-annual variability of gross primary production and ecosystem respiration in a floodprone river during a 15-year period, *Freshwater Biol.*, *51*, 938–950.

Wachniew, P. (2006), Isotopic composition of dissolved inorganic carbon in a large polluted river: The Vistula, Poland, *Chem. Geol.*, *233*, 293–308.

Weiss, R. F. (1974), Carbon dioxide in water and seawater: The solubility of a non-ideal gas, *Mar. Chem.*, *2*, 203–215.

Worrall, F., and A. Lancaster (2005), The release of CO_2 from riverwaters - The contribution of excess CO_2 from groundwater, *Biogeochemistry*, *76*, 299–317.

Worrall, F., W. T. Swank, and T. Burt (2005), Fluxes of inorganic carbon from two forested catchments in the Appalachian Mountains, *Hydrol. Processes*, *19*, 3012–3035.

Yao, W., and R. H. Byrne (2001), Spectrophotometric determination of freshwater pH using bromocresol purple and phenol red, *Environ. Sci. Technol*, *35*, 1197–1201.

Yuan, S., and M. D. DeGrandpre (2008), Evaluation of indicator-based pH measurements for freshwater over a wide range of buffer intensities, *Environ. Sci. Technol.*, *42*, 6092–6099.

C. M. Beatty, M. D. DeGrandpre, L. J. Jungst, J. K. Lynch, and M. P. Seidel, Department of Chemistry, University of Montana, Missoula, MT 59812, USA. (michael.degrandpre@umontana.edu)